In-flight mechanisms in Suspension Plasma Spraying Issues and perspectives

V. Rat, C. Chazelas, S. Goutier, A. Keromnes, G. Mariaux, A. Vardelle

▶ **To cite this version:**

V. Rat, C. Chazelas, S. Goutier, A. Keromnes, G. Mariaux, et al.. In-flight mechanisms in Suspension Plasma Spraying Issues and perspectives. Journal of Thermal Spray Technology, 2022, 31 (4), pp.699-715. 10.1007/s11666-022-01376-2 . hal-03860806

HAL Id: hal-03860806
https://hal.science/hal-03860806

Submitted on 18 Nov 2022

HAL is a multi-disciplinary open access archive for the deposit and dissemination of scientific research documents, whether they are published or not. The documents may come from teaching and research institutions in France or abroad, or from public or private research centers.

L'archive ouverte pluridisciplinaire **HAL**, est destinée au dépôt et à la diffusion de documents scientifiques de niveau recherche, publiés ou non, émanant des établissements d'enseignement et de recherche français ou étrangers, des laboratoires publics ou privés.

In-flight mechanisms in Suspension Plasma Spraying
Issues and perspectives

V. Rat, C. Chazelas, S. Goutier, A. Keromnes, G. Mariaux, A. Vardelle
Institute of Research for Ceramics IRCER UMR7315, CNRS, University de Limoges, France

Abstract

Suspension Plasma Spraying (SPS) has aroused much research efforts over the two last decades to describe and understand the in-flight mechanisms of suspension plasma processing by developing advanced diagnostics and models. This research field has highlighted the intricate and prevailing dependence of the coating properties, and especially the rich variety of attainable microstructures, on the thermal and dynamic histories of the submicron particles in the plasma jet. This paper gives an overview of the major key points to control from the plasma torch operation up to the coating build-up. The main diagnostics methods are examined and the most advanced models as well. The perspectives focus on the key issues to improve the basic understanding of the in-flight phenomena. They also insist on a necessary multiscale approach to combine the diagnostics and the models in order to form relevant data flows for machine learning algorithms and better process prediction and reliability.

Key words: Suspension plasma spraying, in-flight phenomena, diagnostics, models, plasma torch

Introduction

About two decades ago, the ability of Suspensions Plasma Spraying (SPS) process was shown to construct a multiscale coating with a thickness of a few tens or hundreds of micrometers and nanometric features, which improve the coating properties. The outright use of nanopowders injected in a thermal jet has coped with the requirements, first to reach deposition rates as high as in conventional spraying of micrometer particles, and second to avoid the agglomeration of particles. Therefore, a suspension has three main purposes, namely trapping the particles with low inertia, ensuring their efficient dispersion and reaching similar mass flow rates as in conventional plasma spraying. After proper injection, plasma processing of suspensions results in the coating formation, which growth relies on the complex dynamics of impact and flattening of small molten particles that are trapped within the plasma streamlines at the immediate

vicinity of the substrate. Given the particle size distribution of injected particles is usually close to or lower than one micrometre, the lamellae formed after molten particles impact have typical diameters ranging between 0.1 and a few µm while their thicknesses may vary between 20 and 300 nm conferring to the coating some nanometric microstructural features (Ref 1–3). The understanding of the growth mechanisms of coatings has aroused much attention because 1) the latter offer several typical microstructures different from those obtained with conventional Atmospheric Plasma Spraying (APS) and 2) they have allowed improving the Thermal Barrier Coating (TBC) performances due to the combined effect of their columnar microstructure and porosity content (Ref 4). The SPS microstructures span from homogeneous to columnar morphologies. The last category gives rise to typical cauliflower shaped coating architectures with some differences linked to the column width and the inter-column voids, i.e. porous feathery, puffy, narrow and wide columnar (Ref 4,5). The formation of segmented lamellar structures is also reported; it is promoted by the combined effects of high surface temperature and steep temperature gradients through the coating (Ref 5). The homogenous coatings refer to as granular (Ref 1) or to lamellar (Ref 2,3,6) microstructures.

The rich variety of attainable microstructures attracts attention in terms of thermal and mechanical properties but also poses a significant challenge to investigate the mechanisms of coatings growth. First, this is because the particles number per unit time conveyed by the plasma and participating in the coating growth can exceed 10^{10} part/s considering a typical suspension flow rate of 20 mL/min and powder load of 20 wt% for micron-sized particles (1 µm in diameter). Second, the substrate presence and its effect on plasma fluid dynamics are perceived by the molten particles within only the last ten millimetres before impact depending on their Stokes number $S_t = \rho_p d_p^2 v_p / 18 \mu_g \ell$ where ρ_p, d_p, v_p, are the particle density, diameter and speed, respectively, and μ_g,and ℓ the dynamic viscosity of the plasma gas and thickness of the substrate dynamic boundary layer (Ref 7). From the suspension injection point, situated either at nozzle exit or even inside the nozzle for an axial injection, up to the substrate position, the solid particles, initially confined and dispersed with the liquid phase, experience acceleration and heating that result from the successive stages of liquid fragmentation and evaporation, and possibly coalescence of molten particles.

The coatings morphologies and features have a complex multi-parameter dependence including the particle dynamic behaviour in a disturbed flow region close to the substrate at microscopic scale and the coating construction that results from the collective stacking of particles. The suspension properties associated with the in-flight phenomena initiated by the plasma govern

the entire thermal and dynamic history of particles before their impact upon the substrate. Consequently, in the following, an overview is given about the successive stages of SPS from the suspension formulation, suspension plasma processing to the coating formation. Attention is paid on the influence of first order operating parameters on these stages. The current most important diagnostic methods and models are also briefly reviewed. Finally, before the conclusion, some perspectives are discussed.

Suspension formulation

The stability of suspensions of submicron particles is ensured thanks to the balance between the interaction forces described by the Derjaguin-Landau-Verwey-Overbeek (DLVO) theory (Ref 8). The latter assumes that the agglomeration of particles is hampered if the repulsive electrostatic forces that are developed upon their surface dominate the short-range attractive London-van der Waals forces between solid particles. When dispersed within water, a surface charge broadens depending on the nature of the oxide particle and pH value due to the formation of ions on the surface: OH^- or H^+. While a non-zero charge surface charge appears, the counter-ions are distributed around the particles to form an electrical double layer. The electrical influence of the latter extends from the particle surface over a typical distance named the Debye length $\lambda_D = \sqrt{k_B T\varepsilon/2e^2 I N_A}$ where k_B is the Boltzmann constant, T the temperature of the suspension, ε the dielectric permittivity of the medium, e the elementary charge, N_A the Avogadro number and I the ionic strength $I = \frac{1}{2}\sum c_i z_i^2$.(c_i being the molar concentration of the species and z_i its charge number). The overlapping of the electrical double layers of two particles results in repulsive electrostatics forces that repel the two approaching particles. Contrarily to the van der Waals interactions, the repulsive forces can be adjusted by the pH and concentration of ionized species in the solvent.

When the electrostatic forces cannot balance the attractive van der Waals force, small amount of polymer can be added into the solvent (e.g. in ethanol). Long polymeric chain adsorb upon the particles surface and dangle out into the solvent forming a repulsive force (known as steric or entropy force) that hinder the formation of aggregates. In weakly polar solvent, a dispersant combining short-range electrostatic repulsion and steric repulsion can be used to stabilize a Yttria Stabilized Zirconia (YSZ) suspension by means of a phosphate ester (Ref 9). The use of a water-based suspension has interesting advantages, namely lower carbon and economical costs. The zeta-potential can be measured and adjusted (>±30 mV) with the pH and an

additional dispersing agent to avoid the agglomeration and ensure the suspension stability (Ref 10). Note that at very short-range, when the distance between particles is a few nanometres, non-DLVO force arises when the liquid molecules are structured into quasi-discrete thin layers. The so-called solvation force has mainly a geometric origin and can be attractive, repulsive or oscillatory (Ref 8). The suspension must have three main characteristics, i.e. high mass load of powder to reach high deposition rate, low viscosity to ease the liquid injection at high speed and reduced pressure injection, and good stability over the deposition time. The latter is obtained by determining the appropriate mass percentage of dispersant, which depends on the specific surface of powder. Sedimentation tests can then be implemented, and the stability efficiency is assessed by means of optical methods based on light scattered by the suspension. Ultimately, the dispersant content can be finely selected by measuring the lowest viscosity testifying a proper flow structuration composed of solid particles with long dangling polymeric chains or by measuring the zeta-potential.

In-flight phenomena

Plasma processing of suspension

When injecting suspension drops within a thermal plasma jet, the liquid carrier must be quickly eliminated by the plasma in order to process the solid particles trapped within it. The energy required to vaporize the typical solvents used in SPS, ethanol and water, is 1.01 and 2.63 MJ per mass unit, respectively. Therefore, considering only the vaporization latent heat for the phase change and a suspension mass flow rate of $3\text{x}10^{-4}$ kg.s^{-1}, a few hundreds of watts are needed to fully vaporize the liquid, which is by far much smaller than the electrical power of a dc plasma torch and represents only a few percent. This low energy efficiency outreaches the scope of the SPS process. It is related to the dominant mechanism of heat transfer in thermal plasma jet occurring at moderate temperature (<15 000 K) (Ref 11), i.e. the convective heat transfer, that leads to solvent vaporization during the time of flight of the drop. The vaporization time τ_v of a drop whose radius varies from r_s to 0 can be approximated by $\tau_v = L_v \rho_s r_s^2/(T - T_S)\kappa N_u$ where L_v, ρ_s, T, T_S, κ and N_u are the latent heat of the liquid, density of the drop, plasma temperature, temperature at the surface of the liquid, plasma thermal conductivity and Nusselt number, respectively (Ref 9). This simplified formula highlights the dependence of the vaporization on the plasma and drop properties but also on the square of the droplet radius. Its means that the initial drop size as well as the liquid fragmentation process

initiated by the plasma has a straightforward impact on the energetic efficiency of SPS. The liquid fragmentation can be assumed complete when the drag force equilibrates the surface tension force acting on a droplet of radius r_d . The variation of the surface energy starting from a drop of r_s radius to form droplets of radius r_d is equal to the work of the plasma drag force applied during the fragmentation time τ_f, so that $\tau_f = 8\sigma(r_s/r_d - 1)/C_D\rho U^3$ where σ, C_D, ρ and U are the liquid surface tension, drag coefficient, plasma density and plasma speed, respectively (Ref 9). The surface tension is a key parameter for fragmentation (72.75 mN.m^{-1} for water and 21.98 mN.m^{-1} for ethanol) and the plasma velocity as well. It has to be underlined that a fast plasma jet favors the liquid break-up but reduces the residence time in the plasma and, so, possibly brings about incomplete solvent vaporization. Despite the non-uniform temperature and velocity of plasma fields, the above-simplified formula makes it possible to hierarchize the dominant processes: the suspension fragmentation time is several orders of magnitude shorter than the vaporization time under typical operating conditions (τ_f ~ µs and $\tau_f \ll \tau_v <$ 0.1ms).

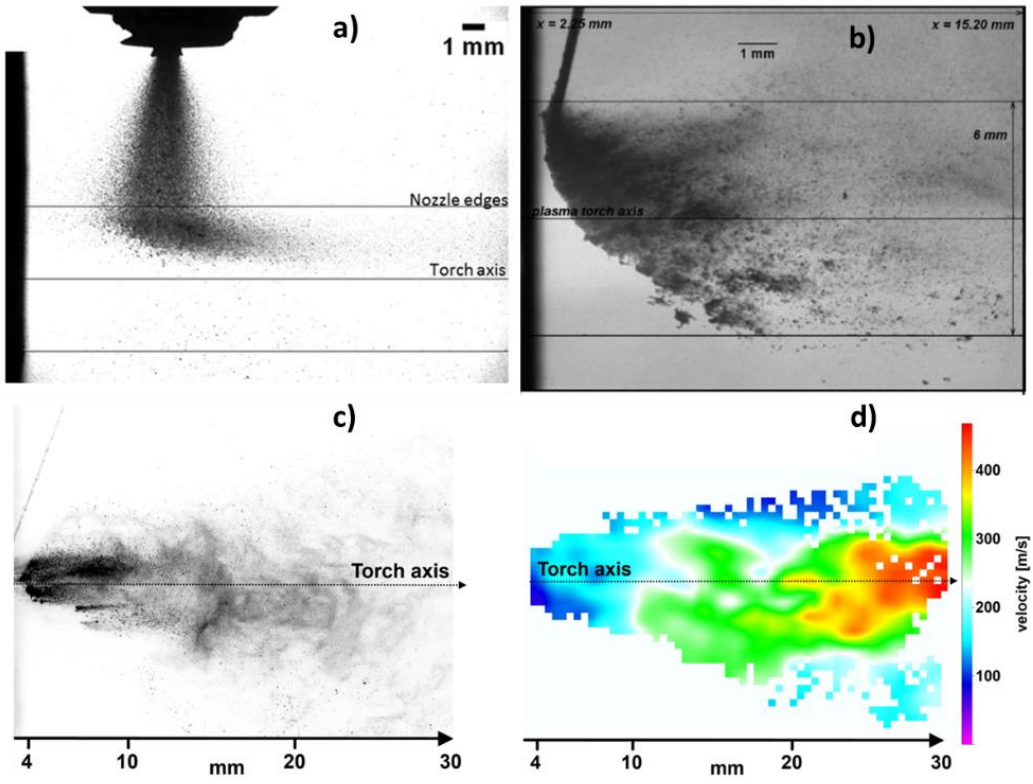

Figure 1 Suspension injection in a dc plasma jet a) Shadowgraph picture of twin-fluid injection (Ref 12) b) Shadowgraph picture of mechanical injection (Ref 13), c) PIV image of mechanical injection, d) velocity distribution.

The residence time of suspension is in the order of about 0.1 ms. The plasma fluctuations are also expected to affect the very fast fragmentation processes. Actually, the typical characteristic times of arc fluctuations may range between a few µs up to hundreds of µs, depending on the arc instability modes (e.g.; restrike, takeover, Helmholtz modes), and the liquid breakup phenomena are triggered by fluid instabilities at the liquid/gas interface.These simple evaluations point out that the liquid does not have a neutral effect on the suspension treatment although its basic function is liquid carrier. This is particularly highlighted in Fig. 1, where the in-flight phenomena are illustrated in shadowgraph pictures taken at the torch nozzle exit.

Figure 1a depicts the suspension injection by means of a twin-fluid atomizer that produces a size distribution of droplets between 10 and a few hundreds of µm (Ref 12) while Figure 1b displays the injection of a liquid column by mechanical injection (Ref 13). The droplet size distribution of the atomizer is controlled by adjusting the gas-to-liquid ratio (GLR, ratio of liquid and gas flow rates) while the liquid column is atomized by the cross plasma jet itself.

The breakup phenomena of drops and liquid columns are classified according to the plasma gas Weber number ($W_e = \rho_p U_p^2 D/\sigma$), momentum flux ratio $q = \rho_\ell U_\ell^2/\rho_p U_p^2$, and Ohnesorge number of drops $Oh = \mu_\ell/\sqrt{\rho_\ell d_\ell \sigma}$ where $(\rho, U)_p$ and $(\rho, U)_\ell$ are the density and relative velocity of the plasma gas and liquid phase, respectively, σ is the surface tension, μ_ℓ the dynamic viscosity of the liquid phase, D is the diameter of liquid column and d_ℓ the diameter of the drop (Ref 14,15). The momentum flux ratio q must be higher than unity to ensure a proper liquid injection within the plasma core and produce an efficient and fast mechanical liquid fragmentation resulting in the so-called catastrophic fragmentation, where $W_e > 100$. The pressure injection, which controls also the liquid mass flow rate of suspension, has to be therefore adjusted to optimize the injection and avoid the travel of fragmentation products at the plasma periphery. The previous non-dimensional numbers offer a relevant guidance to classify the fragmentation modes (Ref 15) or design a shrewd injection device but they implicitly suppose the knowledge of plasma temperature and velocity. The radial injection as depicted in Fig. 1a and 1b brings out the strong dependence of plasma properties on the radial position within the plasma jet. Especially the liquid column starts to be fragmentated in the fringes of plasma due to the large size of the liquid columns (about 200-300 µm) and the temperature dependence of the plasma density which strongly increases at low temperature while the plasma velocity decreases. Therefore, the local Weber number may sharply increase in the plasma fringes as insightfully highlighted by Meillot *et al* (Ref 16). It means that the momentum flux ratio q has to be actually much higher than unity because of this early

fragmentation, which results in an overall decrease of the liquid momentum following the radial distance by reducing the characteristic size of fragmentation products.

In Fig. 1a, the fragmentation of droplets produced by the twin-fluid atomizer is less affected by the high density and velocity gradients in the plasma fringes as the droplet sizes are smaller than that of the liquid column. However, they are more subjected to the drag force and plasma flow instabilities because of their lower inertia. For these reasons the initial liquid elements (large droplet or liquid column) experience a primary fragmentation seeding some liquid fragments which undergo a secondary fragmentation and self-fix the final droplet size distribution (Ref 16) for which W_e becomes small.

Fig. 1c and 1d depict the subsequent treatment of the fragmentation products up to 30 mm from the nozzle exit observed by the Particle Image Velocimetry technique (PIV) for a mechanical injection of the suspension. They highlight the dilution and dispersion of materials, i.e. droplets and particles, which is very non-homogeneous as well as the particle velocity field. Upon the trajectory, the progressive heating by the plasma jet brings about the vaporization of solvent in droplet and the treatment of the submicron particles treatment including their acceleration as shown in Fig. 1b.

Influence of plasma properties

Influence on the suspension injection

When using mechanical injection, the suspension is generally injected radially in the form of a continuous jet or droplet stream. The suspension is introduced into a container connected, via a supply pipe, to the injector placed near the nozzle outlet of the plasma torch. This assembly is pressurized (with air, argon, nitrogen, or helium) and the liquid is injected radially into the plasma jet. Depending on the desired suspension flowrate, the diameter of the injector varies between 150 and 300 µm. As mentioned above, the good penetration of the liquid into the plasma core implies that its dynamic pressure was at least at the same order of magnitude (Ref 17), or even greater, than that of the plasma, i.e. $\rho_\ell U_\ell^2 \geq \rho_p U_p^2$.

The plasma-forming gas composition plays thus an essential role because it governs, through its dynamic pressure, the other parameters being kept constant, the total quantity of precursor injected and, therefore, the theoretical suspension deposition rate. Thus, if the dynamic pressure of the plasma jet is increased, by adding hydrogen or helium, for example, the pressure in the injection system has to be increased, bringing about an increase of the suspension flow rate injected in the plasma jet (Ref 17,18).

Effect on the mechanical and thermal treatment of the suspension

Once the suspension is injected into the plasma core, the latter acts as a source of thermal, chemical and kinetic energy. The first or second mechanical fragmentation of the suspension into drops is therefore the fastest process with respect to the Weber number (We >12) and largely affects the trajectories followed by the drops in the jet, while the evaporation becomes especially significant when the specific surface of the drops becomes large due to the successive fragmentations. It was shown in previous studies using PTF4 plasma torch (Ref 17,18) that shifting from pure argon (33 slpm, $\bar{h}_0$ = 9.16 MJ.kg^{-1}), to argon hydrogen Ar-H_2 (33-10 slpm, $\bar{h}_0$ = 20.46 MJ.kg^{-1}) and to ternary mixtures Ar-H_2-He (45-3-48 slpm, $\bar{h}_0$ =16.5MJ.kg^{-1}) allowed respectively to increase the fragmentation of droplets into smaller drops, despite the fact that the quantity of injected suspension was increased. The plasma jet, at first, acts as an atomizer, whose efficiency depends on its ability to produce rather small droplets with a narrow size range. The chemical composition of the solvent used can also affect both the atomization process and thermal treatment of drops and solid particles. Among other authors, Bertolissi *et al.* and Fauchais *et al.* have showed that the lowest was the suspension surface tension, the smallest were the produced drops (Ref 17,18) in agreement with the Weber number. Ethanol-based suspensions produce finer droplets than water-based suspensions as shown in Fig. 2 where the liquid fragmentation is observed for an ethanol and pure water jet.

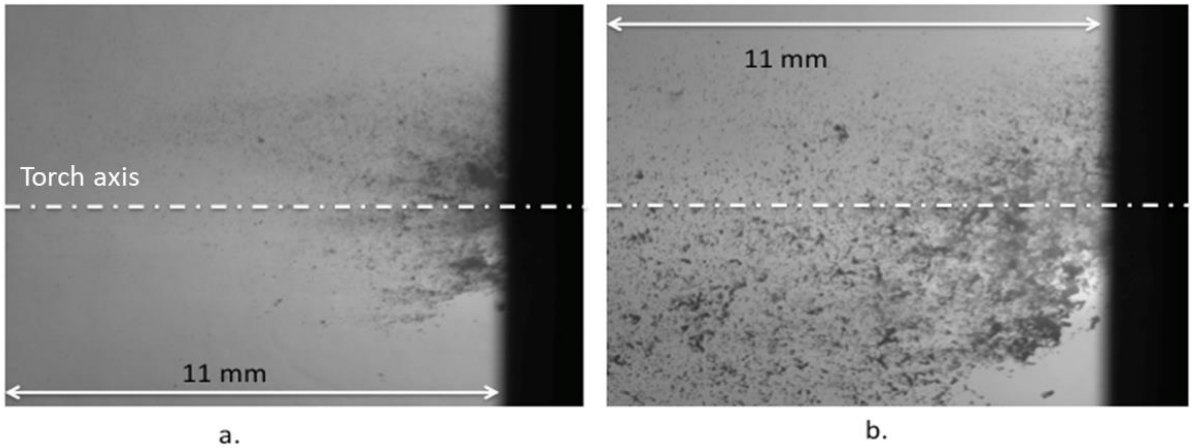

Figure 2 Penetration of a liquid jet injected into the Ar-He (40-20 slpm, h_0 =14 MJ/kg) d.c. plasma jet: a. pure ethanol jet, b. pure water jet (Ref 18)

The chemical composition of the solvent can affect the plasma jet properties and the heating of the drops and particles in the plasma plume. The use of solvents with lower latent heat of evaporation (e.g.; ethanol: 0.84 MJ.kg^{-1} instead of water: 2.26 MJ.kg^{-1}) allow reducing the

plasma jet cooling. Therefore, enough thermal energy remains in the gas to heat the solid particles (Ref 17–19). Figure 3 shows that air injection cooled down the plasma plume while the addition of ethanol enhanced noticeably the temperatures in the plasma plume. Combustion effect between C atoms and oxygen atoms due to air entrainment can be responsible for the temperature increase in the plasma plume. Pateyron *et al.* (Ref 20) also pointed out that if both water- and ethanol-based suspensions hardly modified the plasma viscosity, the thermal conductivity of the plasma was increased by a factor between 2 and 3 in the "newly-formed plasma" due to water and ethanol vaporization. Reactive thermal conductivity presents a maximum at about 3000 K, which results mainly from the decomposition of $H_2 \rightarrow 2H$. The second maximum at about 7000 K can be attributed to the decomposition of $CO \rightarrow C+O$. Pateyron et al introduced the "ability of heating factor" (AHF), a value combining multiple factors related to the plasma/ flame properties. AHF could be increased by a factor between 2 and 3 depending on the suspension based solvent type (water, ethanol or a mix).

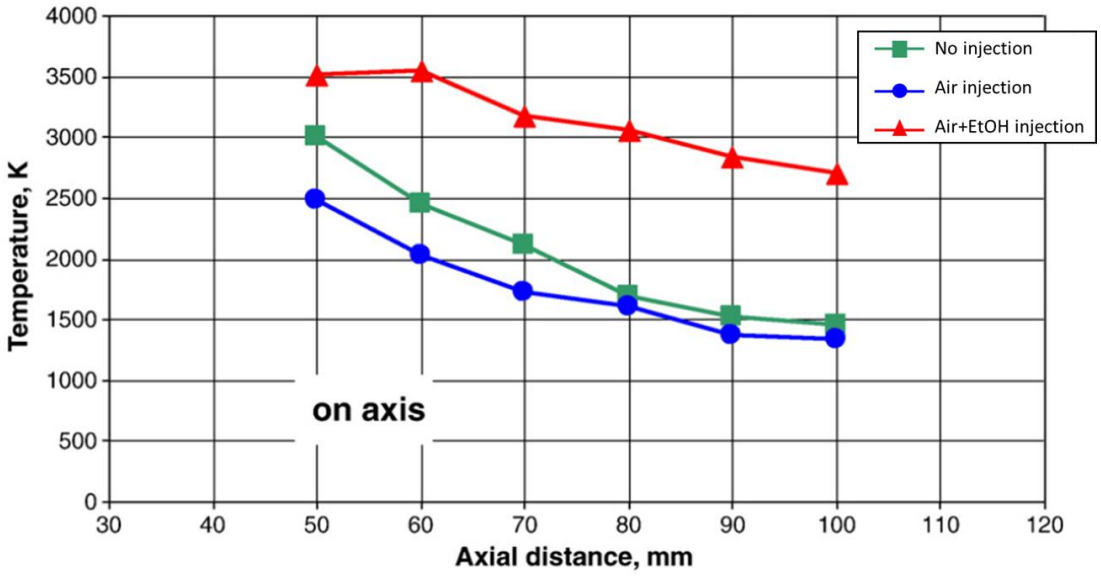

Figure 3 Axial distribution of the measured plasma gas temperatures for three cases, i.e. without any injection, air injection, air + ethanol injection) (Ref 19).

In the same approach, Canas et al. and Cizek et al. (Ref 21,22) have calculated that the AHF increased almost twice when using Dowanol^{TM} (Dipropylene glycol methyl ether) as solvent. They concluded "*such outcome could potentially be exploited in spraying of higher solid load content suspensions, thereby effectively increasing the deposition rates and decreasing the process costs*".

Plasma torches designs and plasma jet properties

The velocity of the plasma jet, via its dynamic pressure ρU^2, directly affects (i) the suspension flow rate, (ii) transverse penetration of the suspension in the plasma jet, (iii) and size of the droplets formed by liquid atomization. It also partly controls (iv) their dwelling time in the hot zone of the plasma jet and capacity to impact on the substrate and, thus, it (v) should affect the deposition efficiency.

Conventional plasma torches, composed of a rod shape cathode and a concentric water-cooled anode, are not well adapted for suspension plasma spraying. Their main drawbacks are the arc root fluctuations on the anode wall when diatomic gas (even 2vol% of H_2) and high gas flow rate of plasma-forming gases are used while the electric power is limited to about 60 kW (Ref 23). These instabilities, although necessary to limit the erosion of the anode, induce temporal variations of arc voltage (up to $\Delta V/\bar{V} > 1$) and temporal and spatial variations of plasma jet velocity, enthalpy and dynamic pressure at the location where the suspension is introduced. For example, when $\Delta V/\bar{V} = 0{,}7$, where ΔV stands for the maximum amplitude of the plasma torch arc voltage and $\bar{V}$ for the mean arc voltage, $\Delta(\rho U^2)$ = 320 % (Ref 24). Thus, the liquid fragmentation after injection depends on the instant when it is injected in the plasma jet. These transient phenomena are detrimental to the reproducibility of the process. Actually, they strongly affect the fragmentation of the liquid jet, and the thermal and dynamic treatment of the suspension drops and particles embedded in the plasma jet.

Plasma spray torches with design different from that of conventional torches are now available on the market. They aim at (i) improving the stability of the plasma jet by limiting the movements of the arc root, (ii) limiting the erosion of the electrodes, in particular of the anode (iii), increasing the length and the specific enthalpy plasma jet and (iv) increasing the throughputs of the processed materials.

To meet the expectations of their customers, equipment manufacturers have developed torches that allow working with a wide range of parameters (electrical power up to 90 kW), high gas speeds, high powder flow rates (greater than 100 $g.min^{-1}$) and lower arc currents. To increase the enthalpy of the plasma, their design favors an increase in arc voltage (with a factor 2 or 3) rather than an increase in arc current, the anode erosion being roughly proportional to the square of the current. To this end, these torches use a cascaded anode made up of a stack of copper rings isolated from each other ("neutrodes") and ending in an anode ring on which the arc is fixed. This design also improves arc stability since the arc movement is limited to the anode

ring. There are a few torches on the market today using cascaded anodes [e.g.; Oerlikon Triplex Pro-210 and Sinplex Pro™ and C + APS from TSD Inc, USA].

Dolmaire *et al.* (Ref 25) studied the propitious effect of hydrogen as plasma-forming gas when using a cascaded (TriplexPro-210, Oerlikon, Kelsterbach, Germany) torch for TBC application. This torch uses three cathodes and the electrical energy is distributed through three parallel arcs striking at a single anode preceded by insulating rings. They showed that adding 10 slpm of H_2 to a 60 slpm argon plasma (arc current intensity of 480A) caused an increase of the $\Delta V/\bar{V}$ value from 5% to 10%. In comparison with a conventional plasma spray torch and identical plasma parameters, the voltage fluctuations increase from 6% to 60%. Without hydrogen in the plasma-forming gas, the ‘‘hot zone’’ lengths are reduced in the range of 70-80 mm. With hydrogen, the plasma ‘‘hot zone’’ lengths are always increasing, up to 130 mm compared to 40 mm for conventional plasma torch.

Same observations can be made when using SinplexPro plasma torch. Its geometry is characterized by a mono-cathode and mono-anode cascaded plasma torch and is thus easier to handle and ensure its maintenance as shown in Fig. 4. The latter depicts the SinplexPro geometry and electrical current density calculated in (Ref 26).

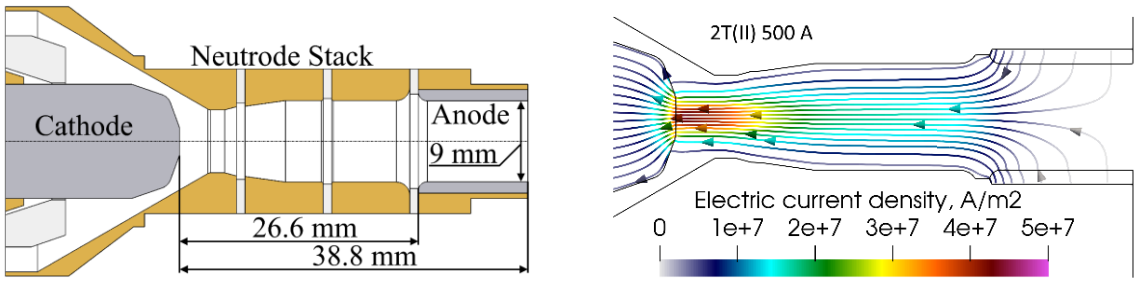

Figure 4 (left) Internal geometry of the SinplexPro™ plasma torch, (right) Instantaneous electric current density streamlines in the gas phase and electrodes, 5.2 ms after the arc ignition; 3D time dependent 2-Temperature model (Ref 26).

Chidambaram Seshadri *et al.* (Ref 27) compared the characteristics of a SinplexPro to a conventional F4MB plasma torch working with Ar-H_2 (50-6 slpm) mixture at the same power level of 35 kW (93V and 380 A for SinplexPro and 65 V and 550 A for F4MB plasma torch). Under these operating parameters, the arc voltage fluctuations $\Delta V/\bar{V}$ of the conventional torch were close to 110% compared to 7% for the cascaded torch. As for Triplex plasma torch, the plasma hot zone is very sensitive to the hydrogen content in plasma-forming gases and can reach 130 mm for adequate operating parameters (Ref 28).

In the previously described plasma torches, solid or liquid feedstock are introduced radially into the plasma jet. They can also be axially injected in the Axial III torch from Northwest Mettech Corp. It is composed of three cathodes and three anodes operated by three independent power supplies and a nozzle in which the three plasma jets converge. It can be fed with Ar-N_2-He or Ar-N_2-H_2 gas mixtures with a total plasma gas flow rate between 100 to 300 slpm and an electric power level up to 140 kW (I = 300-750 A). The feedstock (powder or liquid) is injected axially between the three plasma jets converging within an inter-changeable water-cooled nozzle. Zimmermann et al. (Ref 29) recently experimentally studied the operation of an Axial III^{TM} spray torch. They showed that the plasma jet is characterized by substantial inhomogeneities in the spatial distribution of temperature. Indeed, each of the three plasma torches oscillates as a conventional plasma torch, and the natural fluctuations are not entirely equalized by merging the three plasma streams. The three expanding jets merged only at 30 mm distance to the nozzle exit where the plasma has already cooled down considerably. At last, Xi *et al.* developed a bi-cathode plasma torch operated at low pressure (down to 200 mbars) associated with an axial injection of suspension (Ref 30). They showed that the coating microstructure can be tuned from a columnar to vertically cracked segmented structure by changing the operating pressure.

Coating growth

In a basic configuration of coating deposition where the torch axis is perpendicular to the substrate plane, a stagnation zone is created perpendicular to the fluid flow at the substrate where the axial plasma velocity is vanishing while an accelerating boundary layer is spread out from the stagnation zone along with an increased tangential plasma velocity. The substrate effect experienced by the particles is assessed by means of the Stokes number $S_t = \rho_p d_p^2 v_p / 18\mu_g \ell$ (Ref 7). It can be defined as the ratio of the characteristic time of change of the particle momentum $\tau_p = \rho_p d_p^2 / 18\mu_g$ and the characteristic time during which the flow is under the influence of an obstacle $\tau_0 = \ell / u_0$ where u_0 is the fluid velocity far away from the obstacle. Assuming that the particles tend to the plasma velocity, they are subjected to the presence of substrate as soon as they penetrate the boundary layer of thickness ℓ. For Stokes number below unity, the particles follow the plasma gas streamlines close to the substrate and especially undergo significant deviations from their trajectory initially imparted by the plasma jet. For high Stokes numbers, it is expected that the particles preserve the initial trajectory and collide

more or less perpendicularly with the substrate. The Stokes number shows that small particles are strongly affected due the square dependence of the diameter. Furthermore, the particle speed v_p and the thickness of the boundary layer ℓ are both related to the plasma speed and properties (composition and viscosity). Assuming a constant mass flux density, the mean plasma speed $\bar{u}$ at nozzle exit is simply approximated by $\rho\bar{u} = 4\dot{m}/\pi d^2$ where ρ, $\dot{m}$ and d are the plasma density, mass flow rate of plasma-forming gases, and nozzle diameter, respectively. Instead of using the plasma density, it can be rewritten as $\bar{u} = \bar{h}_0\dot{m}(\gamma - 1)/P_a S\gamma$ where γ, S and P_a are the isentropic exponent, nozzle cross section, and pressure at nozzle exit (Ref 31), respectively. It determines a direct dependence on the mean specific enthalpy $\bar{h}_0$ of the plasma torch and in turn on the momentum gained by particles. Moreover, the thickness of the boundary layer ℓ is expected to decrease with an increase in the plasma speed resulting in a higher Stokes number. It has to be noted that Jadidi *et al.* adopted a different definition of the Stokes number where $\tau_0 = d/u_0$ (Ref 32). For Mauer, it depends on the local curvature of the streamline κ_g close to the substrate where $\ell = 1/\kappa_g$ (Ref 33). The definitions are equivalent at least to give an estimation of the Stokes number. If d is decreased, the plasma speed is increased. It results in increasing the local curvature of the streamline close to the substrate and in decreasing the thickness of the boundary layer. Consequently τ_0 is decreased in any case.

As a result, it is expected that an increase of the plasma speed will favor the increase of the perpendicular component of the particles at the expense of their tangential component with respect to the substrate plane. The particles will contribute to the coating growth following the perpendicular or tangential direction. The rate of increase of the thickness h of the columnar coatings is related to $v_\perp = dh/dt$ and compete with the rate of increase of the width of the columns D, $v_\parallel = dD/dt$ (Ref 4) leading to different coating morphologies. Three main domains are identified in the coating columnar morphology: 1) at the bottom of the coating in connection with the substrate, a region of a few µm in thickness where the columns are initiated from nucleation sites, 2) a region where the columns are developed and 3) at the coating surface top, the heads of the columns where their width can be measured. Depending on the spraying parameters, particles speeds and diameters, the column widths and inter-columnar voids between columns can be varied given that small particles (St < 1) contribute to increase D (Ref 4). It is worth underlining that the coating growth is strongly subjected to the shadowing effect that may be enhanced by the substrate asperities, roughness, stack defects that even may give rise to secondary columns or columns with reverse cone shape.

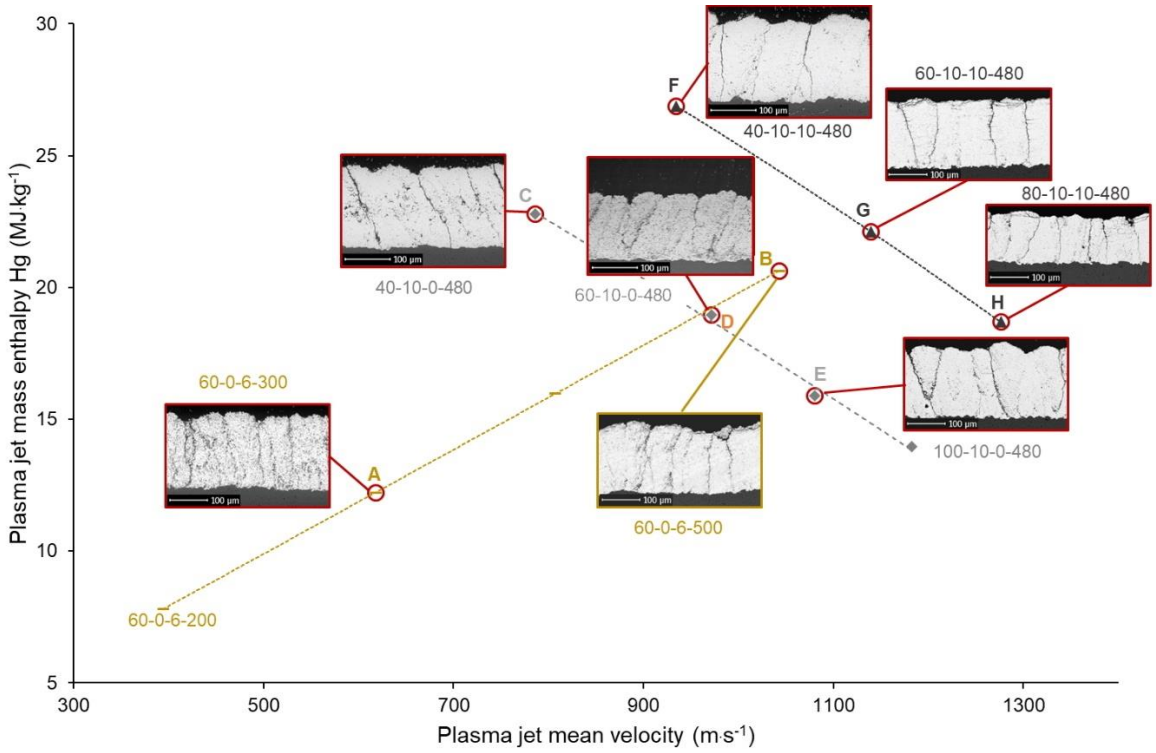

Figure 5 Dependence of SPS coating microstructure on specific enthalpy and mean plasma velocity. The legend refers to Ar-H_2-He-I respectively in slpm for plasma forming-gases and in Amps for the arc current I (Ref 25);

At the immediate vicinity of the substrate (about 100 µm) the particles close to the axis impact upon the substrate with typical velocities of 100 $m.s^{-1}$ while the particles in the periphery have a velocity twice higher but with an incidence angle higher (Ref 34). The angle of column growth is shown to be tightly linked to the incidence angles of particles. Moreover, particles with diameters higher than around 0.7 µm contribute to the coating growth while the smaller ones do not form splats due to a too low impact pressure (<10 MPa) to balance the capillary force and form splats (Ref 34).

Figure 5 highlights the microstructural dependences of SPS coatings on the mean specific enthalpy and mean plasma velocity (Ref 25). The width of the columns increases as the specific enthalpy increase. At low enthalpy (< 15 $MJ.kg^{-1}$), porous and narrow columns are obtained while denser and broader columns are formed at higher enthalpy (> 15 $MJ.kg^{-1}$) and plasma velocity. Variations in plasma-forming gases, flow rates and arc current made it possible to establish a plasma enthalpy/velocity mapping. Note that the definition given to the columns slightly differs between (Ref 4) and (Ref 25) since for the former they were initiated from stacking defects of small lamellae and distinguished by intercolumnar voids while for the latter they were separated by vertical cracks.

Diagnostics

The main challenges of implementing diagnostics are to consider the in-flight processes affecting the materials injected as a multiphase system, occurring following large space and time scales and including successive phase changes. In addition to the description and understanding of the fundamental in-flight processes, the diagnostics must propose relevant on-line methods to control the coating construction.

As a result, the plasma and its interaction with the suspension are characterized from the injection location up to the region close to the substrate. They encompass the direct time-resolved observation of in-flight phenomena (liquid fragmentation and particles dispersion in the plasma plume), and the measurements of particle temperatures and velocities.

The shadowgraph techniques are based on the backlight illumination of the liquid jet and embedded droplets using a high-power spot light (Ref 35) or a pulsed Nd-YAG laser (Ref 36). A commercially available system, SprayCam (Control Vision Inc., USA) is available (minimum particle diameter 20 µm, 10 frames/s). To further investigate the interaction between the liquid feedstock and plasma jet, a high-power light source associated with a short time exposition of observation are needed to overcome the plasma brightness and to avoid the saturation of the camera. This technique is used to visualize and understand the atomization and vaporization processes (minimum detected droplet size of about 5 µm) (Ref 37) leading to a vapor cloud. Thus this technique is recommended by many authors (Ref 38,39) to optimize the suspension injection parameters.

In complement to shadowgraphy, Optical Emission Spectroscopy (OES) is relevant to monitor gaseous phases generated from the vaporization of solvent or of solid particles. It interestingly gives the relative intensities of atomic or ro-vibronic excited levels of metallic and molecular species spread over the UV-VIS-NIR spectrum. Straightforward comparisons can be made between plasma spectra measured without any injection and with suspension injection considering different solvents (e.g.; water and ethanol). The peaks of emission lines corresponding to plasma gas species show smaller intensities if the YSZ suspension is injected (Ref 9,19,40). Since the plasma gas flow rates and thus the concentrations are the same, the gas temperature is lowered by the particle injection highlighting a loading effect on the plasma due to the suspension injection. The liquid evaporation consumes the plasma energy reducing strongly the plasma temperature as shown by Fazilleau *et al.* where the plasma temperature was measured from the oxygen atomic excited lines produced from water evaporation (Ref 9).

When injecting suspension, the spectral analysis points out the existence of evaporated YSZ material. The particles consume part of the plasma energy for heating up and even for evaporation as confirmed by the spectral Zr and Y peaks (Ref 19). The significant existence of YSZ vapours gives evidence of an optimized suspension injection for the applied operating experimental conditions meaning that small particles are properly introduced and kept effectively in the hot plasma core. However, this non-thermal radiation produced by the vapor surrounding the particles is the main source of error in the measurements of particle temperatures (Ref 40).

The quantitative measurement of the plasma gas temperature with injection (solvent alone or suspension) gives rise to some difficulties like the inhomogeneities of plasma at the injection point due to the local cooling. It results that the Abel inversion cannot be used to obtain the temperature profiles (Ref 9). Further downstream, after recovering the symmetry in the emission profiles, plasma temperature can be obtained from a Boltzmann plot or a relative atomic line intensities method of plasma gas species. The lines of latter must not overlap with the YSZ excited species, their energetic gaps must be significant (> 2-3 eV) and they must not be drowned in the continuum background radiation (Ref 41). The atomic lines intensities obviously decrease as the distance from the nozzle diminishes and overlap with emitting molecular systems (e.g. OH, CN, N_2, N_2^+, ZrO, …) for T<6,000 K due to the evaporation, the possible combustion of the solvent, the air mixing and the oxidation of metallic vapours (Ref 41,42). The concentration of metallic atoms in their fundamental state can be deduced from the measurement of the excitation temperature vitiated by a substantial error ($\pm$20%) (Ref 41) or from absorption spectroscopy (Ref 43) which has not been applied yet to SPS to the best knowledge of the authors.

The temperature and velocities of the particles are measured by means of the AccuraSpray (Tecnar) which a recent new version has been developed in order to face the challenges posed by SPS, especially the important temperature gradient along the spray axis (Ref 44). To solve this problem, a single-point measurement system has been developed in an updated version called AccuraSpray 4.0. The radiation emitted by the particles in the measurement volume is captured in one point and the collected signal is split and filtered in order to reach the detectors at two different wavelengths. To prevent any stray radiation from the plasma jet, filters have been added. The temperature measurement is based on the two-color pyrometry principle. This temperature represents an ensemble measurement, i.e. the average temperature of the particles crossing the measurement volume, approximately 150 mm^3. The device also measures the velocity of in-flight particles based on the time-of-flight technique. It

has to be underlined that the calculated temperature is quite sensitive to the stray radiation from the plasma jet at low standoff distance (30 mm) but this effect tends to be reduced at further distance. However, no noticeable impact on the velocity accuracy has been observed. So far, this recent device has been used in two different studies dealing with suspension (Ref 45,46). Cizek *et al.* measured the temperature and velocities of the particles at a stand-off distance of 100 mm, whereas Yvenou *et al.* pointed out the difficulty to measure the particles temperature due to the high luminosity of the plasma jet at a shorter distance (between 5.3 cm and 6.3 cm), but measured the particle velocity.

The PIV technique permit to track very small droplets or particles down to about 50 nm. It has been widely used to spatially characterize fluid flows over the last four decades (Ref 47). However, the use of PIV in SPS is quite recent (Ref 48). It is a non-intrusive technique based on the double illuminations of particles in fluid by a laser sheet. Light scattered by the particles is captured by one or two cameras. During PIV measurement, it is necessary to drastically reduce the exposure time (down to 50 µs for Chen *et al.*(Ref 49)) and use a band-pass filter to reduce the effect of the bright plasma plume. Therefore, standard double-shutter PIV cameras cannot be used due to the long exposure time. A cross-correlation algorithm calculates the displacement of the particles between the two images and the velocity field can be obtained knowing the time difference between the laser pulses. In their work, Marchand *et al.* studied the interaction of the suspension with the plasma flow (free jet) and highlighted the importance of the particle velocity when penetrating the plasma jet. They also noticed an important difference between the velocities measured by PIV and AccuraSpray 3.0, respectively 210 $m.s^{-1}$ and 430 $m.s^{-1}$ at a spray distance of 40 mm. Using PIV, Chen *et al.* (Ref 49) studied the atomization process and droplet velocity distribution in the plasma plume and compared the velocity distribution and fragmentation in the plasma jet for two plasma conditions. More recently, Dolmaire *et al.* (Ref 34) studied the effect of the substrate on the particle velocities, and especially in the stagnation zone closed to the substrate (0.2 mm), in order to emphasize the role of the smallest particles (below 0.7 µm) on the formation of multiscale porosity.

The diagnostics of particles of a few tens of micrometers at impact upon the substrate made is possible to investigate their conditions of flattening and coating formation according the operating parameters (Ref 50–55). The experimental arrangement combines time-resolved imaging and fast pyrometry of individual particles operating at time and space scales of a few microseconds and of few tens of microns, respectively. However, for the SPS process, the observation of particle at impact remain challenging due to their very fine size. Consequently, to circumvent this problem, a non-dimensional approach can be used in order to obtain as much

as possible the same impact condition (Ref 56). Complementary analyses of particle flattening can be performed by means of Atomic Force Microscopy and Focused Ion Beam at microscopic scale (Ref 57).

Modelling

At present, none of the diagnostic systems makes it possible to provide distribution of velocity, temperature, molten/liquid state, and size of the droplets and/or particles just before impact on the substrate. These distributions are essential to understand, control and even predict the coating growth. Reliable models could usefully complement the information provided by the diagnostics. They should help (i) to understand the material processing and its interaction with the flow and (ii) study the effect of operating parameters on the particle properties distributions at impact.

The SPS process includes different sub-systems:

1. formation of the plasma in the torch,
2. development of the turbulent plasma, mixing with ambient gas and interaction with substrate,
3. injection, fragmentation and processing of the suspension in the plasma jet and close to substrate;
4. relative movement of the torch in relation to the substrate.

The latter should be particularly considered for up-scaling purposes from the laboratory to the industry.

Most of current models include the subsystems 2 and 3. They consider gas velocity and temperature profiles at the torch nozzle exit drawn from experimental measurements or from enthalpy and mass flow balances at nozzle exit. A few include also the formation of the plasma jet in the torch. The latter can be simulated either by solving the Navier-Stokes and energy equations with the addition of a source term in the energy equation to model the conversion of electric energy to gas enthalpy (Ref 58,59), or by solving the Navier-Stokes and energy equations coupled with the Maxwell electromagnetic equations. The most advanced plasma torch models are 3D and time-dependent as the suspensions are very sensitive to the plasma jet fluctuations (Ref 60). They take into account the nonlocal thermal equilibrium (NLTE) close to the electrodes by using a two-temperature model (electrons and heavy species) and a cathode

sheath model (Ref 61); they also include the electrodes in the computational models (Ref 62–64) and solve the energy and electromagnetic equations in the gas phase and electrodes.

However, if these models yield more reliable and realistic data, they are not used in the simulation of suspension processing yet. Actually, they are resource and time-consuming, and generally require the implementation of specific models and numerical tricks that are not readily available in the commercial codes used for the numerical simulation of suspension processing. A solution would be the linkage of the code used for the electric arc model to a CFD code that makes it possible to calculate the plasma flow issuing from the plasma torch nozzle and treatment of the suspension in the gas flow. This code would use as boundary conditions at the nozzle exit the output variables of the arc modeling with an iterative or non-iterative linkage procedure depending on the stability of the plasma torch.

The development of the plasma jet issuing from the torch is usually modeled by solving the conservation equations for a LTE non-reactive multi-species gas mixture (plasma gas, ambient and evaporated liquid ones). The fluid is assumed compressible (Mach 0.3-0.7) (Ref 65) or incompressible, in steady or unsteady state. 3D calculation domains are considered when the suspension is injected radially in the plasma jet and also consider a substrate that may have a particular shape. The turbulence is usually modeled with time-averaged turbulence models (Reynolds Averaged Navier-Stockes, RANS) that has the main advantage to use limited CPU resources (Ref 66,67). Nevertheless, these models do not represent the development of transient and small turbulent structures and may underestimate both the gas temperature and its mixing of plasma with the ambient gas (Ref 66,67). Direct Numerical Simulation is not accessible yet because of the high Reynolds number of such plasma flows. However Large Eddy Simulation models (LES) using reasonable cells number (about 500,000 to 1 M) have been used in a few cases (Ref 65,68,69) with time-dependent boundary conditions at the nozzle exit. They reveal a larger range of turbulent scales than the RANS models. Actually, the LES turbulent viscosity represents the dissipation in the un-solved parts (sub-grid) of the flow whereas the RANS turbulent viscosity represents the dissipation in the whole grid.

The processing of the suspension involves several stages. They include the injection under the form of liquid jet (mechanical injection) or droplets (atomizer), primary fragmentation of the liquid jet and secondary fragmentation of droplets, solvent evaporation with potential deformation of droplet (Ref 70), agglomeration (or eventually dispersion) of the primary suspended particles, consolidation of particles, melting with possibly evaporation of the liquid phase and possible re-condensation. In the case of mechanical injection, the cross-plasma jet provides the atomization of the liquid jet. Its fragmentation depends on the development of

Kelvin-Helmholtz waves by Rayleigh-Taylor instabilities due to the liquid-gas interface shearing and depends on the Weber number. The most adapted model should use a fluid tracking surface approach, as the Sub Mesh Volume of Fluid method (VOF-SM) proposed by Vincent and Caruyer (Ref 71,72) with the CFD Aquilon code. However, this approach requires a very fine mesh grid and is still limited to a zone close to the suspension injection orifice. Therefore, in most of the studies, a Lagrangian approach is used for the droplets and particles released by the droplet evaporation. The primary fragmentation is usually represented by the injection of a train of droplets with a diameter similar to that of the injector (Ref 60,73). The secondary break-up of these droplets are modeled by phenomenological models (Ref 60,73–75) depending on the Weber number like the Taylor Analogy Break-up model (TAB), Enhanced Taylor Analogy Break-up model (ETAB), Wave model and the KHRT model that combines the Kelvin-Helmholtz (KH) waves and the Rayleigh-Taylor instabilities on the droplet surface. They predict the droplet size distribution, positions and initial velocities. According to Gulyaev (Ref 76), the liquid evaporation proceeds after complete liquid breakup and droplet spheroidization that are almost instantaneous (10^{-9}–10^{-7} s), so that the fluid properties (viscosity, surface tension) remain almost constant during the breakup stage.

The droplets are accelerated by the gas flow mainly under the action of the drag force and subjected to thermophoretic forces when their size decreases (Ref 77). In most studies, a perfect sphere shape is assumed but due to the droplet distortion it can evolves from a sphere to a disk and the drag coefficient should be dynamically changed according to a damped force oscillator equation giving the droplet distortion (Ref 60).

The suspension droplet is generally modeled according to the “multicomponent approach” (Ref 60) for which the solid concentration and temperature are assumed to be spatially uniform (the Biot number is usually low). This solid concentration increases until the total evaporation of the liquid; one droplet produces then one spherical particle assuming that all the submicronic suspended particles agglomerate.

Generally, the physical properties (density, viscosity, heat capacity, surface tension) of the liquid are assumed constant and equal to that of the pure liquid during the evaporation stage, even if the solid concentration changes and the liquid properties can vary by about 10-20% (Ref 77). However, the change in particle concentration affects the drying rate via the liquid vapor diffusivity. In addition, the liquid evaporation changes the composition of the continuum phase and should be considered through source terms in the gas conservation equations as well as in the thermodynamic and transport properties of the gas mixture. Assuming that no chemical

reactions take place in the gas phase, the latter can be calculated by using mixing laws depending on the vapor concentration (Ref 60).

The heat transfer between the gas and droplets/particles proceeds mainly by convection. The transfer coefficient expressed through the Nusselt number should be corrected to consider the variations of physical properties in the boundary layer that develops around particles and rarefaction effects. It should also consider the effect of the intense evaporation of liquid (Ref 77,78). Similarly, the drag coefficient must be corrected to account for the same effects.

As soon as the solvent is fully vaporized, the particles are heated, molted and possibly vaporized. Figure 6 shows the predicted temperature field of a plasma jet issued from a commercial SG-100 plasma torch and particle temperature distribution at three different instants of time.

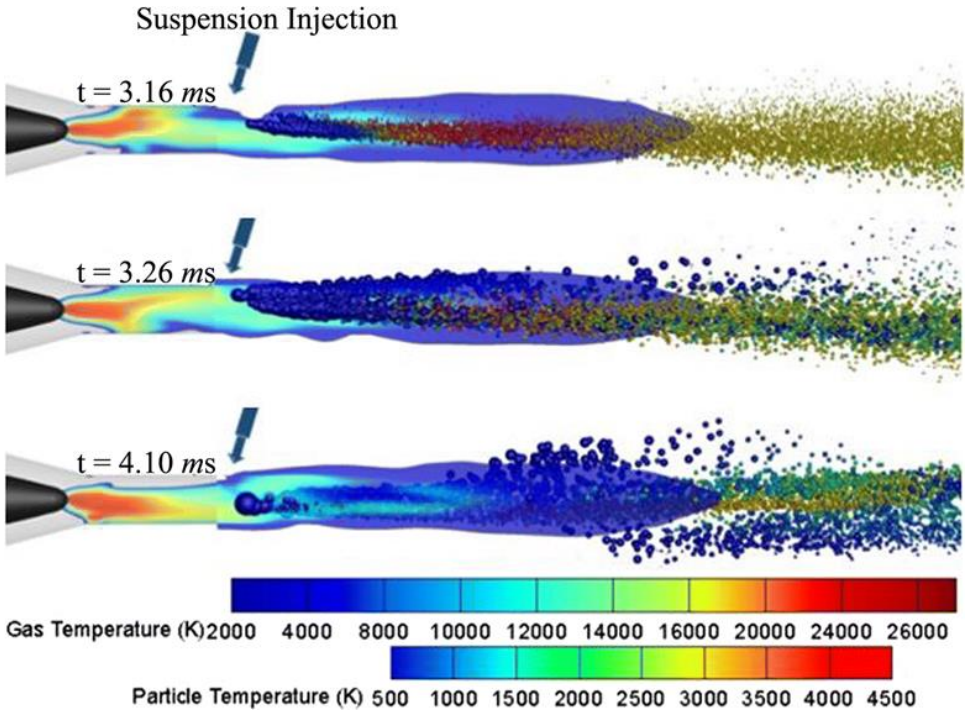

Figure 6 Plasma gas and particle temperature distribution at three different instants of time from Dalir et al, Modeling of Suspension Plasma Spraying Process Including Arc Movement Inside the Torch (Ref 73).

According to the Biot number of ceramic materials, the temperature in the particles cannot be longer considered as homogenous. 1-D heat model considering the temperature gradient and the melting and evaporation front should be used even it is not often the case yet (Ref 79).

If most of the models follow the previous approach, questions arise about the internal circulation in the droplet and the redistribution of the suspended particles in the droplet. Indeed,

for high gas-droplet heat transfer rate, the submicronic particles do not have enough time to redistribute by themselves by diffusion (Pe >>1). This point was recently addressed by Javid *et al.* (Ref 70,80) that developed a 2D axisymmetric numerical model of the successive stages of the agglomeration process during buckling including droplet shrinkage, shell formation, buckling and cavity growth in the droplet. This model makes it possible to predict the droplet shapes that are experimentally observed.

Discussion and perspectives

The control and improvement of SPS coating properties can be strengthened by alleviating the influence of major sources of instabilities affecting the different stages of the suspension processing. It mainly relies on the synergistic effects between the plasma torch and injection technology. On the one hand, the torch design and operating parameters govern the plasma stability, its properties and their respective gradients. On the other hand, the injection technology, producing a liquid column or a droplet spray and fixing the suspension mass flow rate, affects the suspension processing whose fragmentation processes are triggered by fluid instabilities. Consequently, it can be expected that the suppression of the primary liquid fragmentation would be interesting to mitigate a disordered fragmentation. It results that an axial injection mode of a calibrated droplets spray would be efficient to avoid the mechanical barrier formed by the increase of plasma density (increase of W_e) in the plasma fringes when the radial injection is used.

The Axial III torch allows the axial injection by means of the combination of three conventional torches. However, the arc instabilities still remain (Ref 29). Even though the latter can be expected to be smoothed in the three merging plasma jets, the inhomogeneities of the spatial distribution of plasma properties may affect the suspension processing due to the low fragmentation and evaporation characteristic times. This issue could be circumvented by the association of cascaded anode plasma torches but it represents a substantial technological challenge. Note that the radial suspension injection can be perturbed by the extension of electrical current lines outside the nozzle channel (Ref 81) which can be promoted by the use of cascaded plasma torches. It is worth mentioning that, in case of the increase in suspension throughput for productivity purposes, the torch electrical power has to be increased to yield a broader plasma volume available but this can be detrimental to the electrode durability.

A high liquid fragmentation efficiency requires a high dynamic pressure of the plasma ρU^2 (W_e > 100) while fast evaporation needs a high plasma enthalpy $\bar{h}_0$. However, the plasma density ρ decreases with $\bar{h}_0$. It means that a high enthalpy $\bar{h}_0$, often linked to a high electrical power, leads to opposite effects on fragmentation and evaporation. This is because the plasma velocity is intimately linked to the specific enthalpy through the specific volume that increases as temperature rises. Moreover, the plasma viscosity increasing with $\bar{h}_0$, at least below 10 000 K, the mixing of the small particles with the plasma is more difficult.

It results that the droplets should be conveniently injected axially with the lowest droplet size distribution (with low W_e) in the plasma core to favor an efficient evaporation and subsequent particles mixing with the plasma for a better heat transfer. However, the solvent vaporization can also be a thermal process that complete the fragmentation at very low Weber numbers (Ref 42). Starting from a spherical droplet, this thermal fragmentation or explosive vaporization may form some kind of ligaments composed of vapor or liquid spreading at counter flow in the plasma jet. The assumption of spherical evaporation is in particular questioned owing the non-uniform plasma heating that induces first different evaporation rates upstream and downstream of a single droplet and second a high-pressure gradient of steam at its interface (Ref 82). Moreover, the pressure difference is sufficient to overtake the capillary force and deform the droplet.

A refined description of the evaporation of the liquid is of major interest not to skew the interpretation of the subsequent plasma treatment of solid particles. Considering that the main purpose of SPS is to construct finely-structured coatings embedding additional features at nanometric or sub-micrometric scale, the submicron size of particles should be conserved during their flight. However, some experimental studies report that submicron particles may experience coalescence to form larger particles (Ref 1). It can be inferred that during the evaporation of the solvent, the effective dispersion between submicron particles is curbed until the particle agglomeration finally occurs. The consolidation of agglomerates probably results from the plasma heat transfer leading to melting and coalescence. The sintering stage of solid particles is unlikely due to much higher characteristic times (> 1ms) and absence of external applied pressure.

However, very fine particles are also collected suggesting that single submicron particles can be sprayed or result from some agglomerates which are disassembled in-flight (Ref 1). It is worth underlining that the control of plasma treatment of agglomerates of nanoparticles is challenging because they result in large particle size distribution due to the agglomerates

dismantled by the plasma. This uneven explosion of agglomerates was also shown to be linked to the instability of the plasma while a monodisperse initial particle size distribution without agglomeration should be privileged (Ref 1). The potential scenarios of suspension treatment described for example in (Ref 1,83) also depend on the particle size distribution, mass load, and solvent nature (organic/non organic) on which depend the suspension stability and particle agglomeration.

As explained in the section "Suspension formulation", the stability of suspensions is a key issue in the SPS process and is inevitably affected either by the chosen powder mass load required to reach significant deposition rates or simply by aging effects of the suspension. It results that the particles agglomeration and sedimentation must be avoided as mentioned by appropriate suspension properties. However, the viscosity and the surface tension directly influence the droplets size distribution during primary and secondary fragmentations. The droplet sizes are shown to be reduced as the viscosity and surface tension are decreased leading to smaller molted particles and to more columnar and porous coatings (Ref 84,85). It has to be underlined that the axial injection in Axial III plasma torch seems to be less dependent on the suspension properties and is a field of investigation of research and technology for an optimized injection (Ref 85).

Note that when the evaporation of the solvent is uncompleted, it can be expected that the solvent evaporates on the substrate whose temperature is higher than 400°C leading to some porosity in the coating and/or in some disorder in the columns that grow from the substrate surface and form the coating.

A better understanding and description of particle agglomeration during the evaporation stage is necessary not only to account for more realistic assumptions in models but also to control the agglomerate formation and their possible in-flight dismantling. As shown above, when using the Stokes number to interpret the coating growth, the particle size distribution is essential but the analysis implicitly assumes a viscous flow regime ($St<1$) for small particles. Questions may then arise in the light of Fig. 1c where turbulence may be enhanced due to plasma flow instabilities, and presence of small particles and even nanoparticles possibly formed from material vapors (Ref 67). To exploit the potentials of such novel plasma spray processes like SPS, the plasma-feedstock interaction must be understood better. In particular, the decomposition and evaporation of feedstock material during process is interesting to investigate since the material processing stages affect the deposit properties like stoichiometry, and structural and microstructural features (Ref 3,19). Furthermore, a particle loading effect exists as reported in (Ref 40,86). The evolution of the size distribution of in-flight particles, from the initial powder of the suspension up to the particles really contributing to the coating build-up,

brings about major challenges in terms of diagnostics methodology and sensors capabilities (pixel size, CCD array size, dynamic range, integration time, signal/noise ratio, …) to effectively capture the phenomena underlaying the coating growth. It results from the large span of in-flight particle size distribution including vapours up to micro-sized particles. Note that VanEvery *et al* (Ref 3) claim that the vapour produced during the process could induce the cauliflower structure of the coating like in EBPVD system. Considering that the particle mass or volume flow rate reflects the coating construction (Ref 87,88), its measurements is based on the intensity I of the thermal radiation emitted by the particles which is diameter d and temperature T dependent ($I \approx d^2T^4$). The signal/noise ratio from the fine particles becomes low whereas they contribute to the coating even with low Stokes number (St < 1) and affect the microstructure. Moreover, due to the low momentum and temperature inertia of fine particles and very large property gradients in the plasma (in the plume or close to the substrate), the diagnostic methodology and volume sensed must be adapted accordingly (Ref 40). At last, active diagnostic methods should be developed to particularly probe the fine particles (~ 1µm) by means of laser diffraction or PIV (Ref 34,89). The influence of plasma radiation and non-thermal radiation from the particle evaporation can be discarded by the use of appropriate laser wavelength, power and time-resolved measurement.

The association of multiple sensors are therefore expected to probe the multiscale particles contributing to the coating knowing that the largest particles influence the mass (volume) flow rate of particles and subsequently the coating thickness, but also the smallest ones which will affect the coating morphology, i.e. the porosity and the columnar microstructure.

In addition to these diagnostics, it is important to establish a link between the data collected and the properties of the coating. A multifactor analysis is then necessary to obtain robust and liable data and thus to increase the performance of the process. The analysis can be performed by implementing an artificial neural network (ANN) structure that implicitly encodes the physical phenomena governing the process. The step-by-step optimization of such a code leads to identify an ANN structure representing the correlations between the processing parameters and the characteristics of the particles in flight (Ref 90–92). Similarly, the construction of the coating is also oriented towards the digital realization of the entire process, including the plasma torch and the robot, in order to optimize its trajectory and reducing the trials number and the experimentation error (Ref 93).

If none of the models integrates all the phenomena that occur in the plasma spray process, the most advanced ones produced realistic predictions that can help to better understand the process (Ref 60,61,71,73). To model the process in a representative way, each

subsystem described in section 5 must be accurately modeled, which will inevitably lead to very heavy numerical simulations. One possible way is to use the best adapted model and code for the simulation of each phenomenon, and to manage the data flow between codes via a digital platform that coordinates the chaining and interaction of the different codes or models. However, this approach requires the upstream parallelization of all the codes and significant computing resources. Another way is the use of a model reduction scheme. The latter is based on the generation of simplified system models with outputs acceptably similar to those of the original system or model. They use little CPU resources and can produce massive data in a reasonable time. This approach is thought to be useful for the application of machine learning to the suspension plasma spray process.

Finally, an essential issue for all the models currently proposed in the literature is the validation of their predictions against reliable experimental data obtained under the same operation conditions and with a similar suspension (composition, size of primary particles, feed rate, etc.)

Conclusion

Suspension Plasma Spraying has emerged for two decades in order to take advantage of nanometric features of materials in coatings. Since then, the SPS coatings properties have shown their interest with respect to APS ones so that the SPS technology is being developed at industrial level. From a phenomenological point of view, the successive stages of mechanical and thermal decomposition of suspension are well described by means of specific time-resolved diagnostics, like imaging, shadowgraphy, PIV, OES. However, owing to their complex implementation, these methods often focus on each stage separately. The same observation can be made for the models which require large CPU resource although the effect of plasma torch fluctuations on suspension treatment has been recently considered (Ref 73).

Actually, the intermediate position of the SPS process between thin film deposition methods (like PVD) and thermal spray technologies gives rise to multiscale difficulties, namely 1) from the short times scales of arc fluctuations or droplet fragmentation (~ µs) to the time of flight of particles (~ 0.1 ms) and 2) from the particle size (≤ µm) to the coating thickness (~ 100 µm). Moreover, the evaporation of the liquid feedstock and possibly of the particles also generate some vapors spreading over the plasma plume. These excited species contained in these vapors contribute to overlap the thermal radiation of particles and disturb their temperature

measurements. Moreover, they could also affect the coating growth to an extent that needs to be examined.

Consequently, the description of SPS phenomena should rely on the combination of complementary advanced models and diagnostics to properly circumvent the complex multiscale effects. It allows refining our overall understanding of SPS to develop on-line monitoring tools grasping the most important data and reflecting the coating properties. The identification of relevant subsystems, the generation and the flow of key data, including their chaining, will permit to feed machine learning algorithms for better process reliability and prediction of coating properties.

Acknowledgement

The authors gratefully acknowledge the CEA, SAFRAN, Nouvelle-Aquitaine region, the French National Research Agency (ANR) for supporting the research projects.

References

1. C. Delbos, J. Fazilleau, V. Rat, J.-F. Coudert, P. Fauchais, and B. Pateyron, Phenomena Involved in Suspension Plasma Spraying Part 2: Zirconia Particle Treatment and Coating Formation, *Plasma Chemistry and Plasma Processing*, Springer, 2006, **26**(4), p 393–414.

2. H. Kassner, R. Siegert, D. Hathiramani, R. Vassen, and D. Stoever, Application of Suspension Plasma Spraying (SPS) for Manufacture of Ceramic Coatings, *J Therm Spray Tech*, 2008, **17**(1), p 115–123.

3. K. VanEvery, M.J.M. Krane, R.W. Trice, H. Wang, W. Porter, M. Besser, D. Sordelet, J. Ilavsky, and J. Almer, Column Formation in Suspension Plasma-Sprayed Coatings and Resultant Thermal Properties, *J Therm Spray Tech*, 2011, **20**(4), p 817–828.

4. B. Bernard, L. Bianchi, A. Malié, A. Joulia, and B. Rémy, Columnar Suspension Plasma Sprayed Coating Microstructural Control for Thermal Barrier Coating Application, *Journal of the European Ceramic Society*, 2016, **36**(4), p 1081–1089.

5. R. Chidambaram Seshadri, G. Dwivedi, V. Viswanathan, and S. Sampath, Characterizing Suspension Plasma Spray Coating Formation Dynamics through Curvature Measurements, *J Therm Spray Tech*, 2016, **25**(8), p 1666–1683.

6. M. Shahien, M. Suzuki, and Y. Tsutai, Controlling the Coating Microstructure on Axial Suspension Plasma Spray Process, *Surface and Coatings Technology*, 2018, **356**, p 96–107.

7. P. Fauchais, M. Vardelle, A. Vardelle, and S. Goutier, What Do We Know, What Are the Current Limitations of Suspension Plasma Spraying?, *Journal of Thermal Spray Technology*, Springer, 2015, **24**(7), p 1120–1129.

8. Y. Liang, N. Hilal, P. Langston, and V. Starov, Interaction Forces between Colloidal Particles in Liquid: Theory and Experiment, *Advances in Colloid and Interface Science*, 2007, **134–135**, p 151–166.

9. J. Fazilleau, C. Delbos, V. Rat, J.F. Coudert, P. Fauchais, and B. Pateyron, Phenomena Involved in Suspension Plasma Spraying Part 1: Suspension Injection and Behavior, *Plasma Chem Plasma Process*, 2006, **26**(4), p 371–391.

10. A. Potthoff, R. Kratzsch, M. Barbosa, N. Kulissa, O. Kunze, and F.-L. Toma, Development and Application of Binary Suspensions in the Ternary System Cr2O3-TiO2-Al2O3 for S-HVOF Spraying, *Journal of Thermal Spray Technology*, Springer, 2018, **27**(4), p 710–717.

11. E. Pfender, Particle Behavior in Thermal Plasmas, *Plasma Chem Plasma Process*, 1989, **9**(S1), p 167S-194S.

12. E. Aubignat, M.P. Planche, D. Billieres, A. Allimant, L. Girardot, Y. Bailly, and G. Montavon, Optimization of the Injection with a Twin-Fluid Atomizer for Suspension Plasma Spray Process Using Three Non-Intrusive Diagnostic Tools, *J Vis*, 2016, **19**(1), p 21–36.

13. E. Meillot, R. Vert, C. Caruyer, D. Damiani, and M. Vardelle, Manufacturing Nanostructured YSZ Coatings by Suspension Plasma Spraying (SPS): Effect of Injection Parameters, *J. Phys. D: Appl. Phys.*, 2011, **44**(19), p 194008.

14. M. Jadidi, S. Moghtadernejad, and J. Hanson, Numerical Study of the Effects of Twin-Fluid Atomization on the Suspension Plasma Spraying Process, *Fluids*, 2020, **5**(4), p 224.

15. M. Jadidi, A. Vardelle, A. Dolatabadi, and C. Moreau, Heat Transfer in Suspension Plasma Spraying, *Handbook of Thermal Science and Engineering*, (Cham), Springer International Publishing, 2018, p 2923–2966, doi:10.1007/978-3-319-26695-4_30.

16. E. Meillot, S. Vincent, C. Caruyer, D. Damiani, and J.P. Caltagirone, Modelling the Interactions between a Thermal Plasma Flow and a Continuous Liquid Jet in a Suspension Spraying Process, *J. Phys. D: Appl. Phys.*, 2013, **46**(22), p 224017.

17. G. Bertolissi, C. Chazelas, G. Bolelli, L. Lusvarghi, M. Vardelle, and A. Vardelle, Engineering the Microstructure of Solution Precursor Plasma-Sprayed Coatings, *Journal of thermal spray technology*, Springer, 2012, **21**(6), p 1148–1162.

18. P. Fauchais, A. Joulia, S. Goutier, C. Chazelas, M. Vardelle, A. Vardelle, and S. Rossignol, Suspension and Solution Plasma Spraying, *Journal of Physics D: Applied Physics*, 2013, **46**, p 224015.

19. G. Mauer, A. Guignard, R. Vaßen, and D. Stöver, Process Diagnostics in Suspension Plasma Spraying, *Surface and Coatings Technology*, 2010, **205**(4), p 961–966.

20. B. Pateyron, N. Calve, and L. Pawłowski, Influence of Water and Ethanol on Transport Properties of the Jets Used in Suspension Plasma Spraying, *Surface and coatings technology*, 2013, **220**, p 257–230.

21. E. Canas, M. Vicent, M.J. Orts, and E. Sanchez, Bioactive Glass Coatings by Suspension Plasma Spraying from Glycolether-Based Solvent Feedstock, *Surf. Coat. Technol*, 2017, **318**, p 190–197.

22. J. Cizek, D. Dukovsky, R. Musalek, J. Medricky, T. Tesar, F. Lukac, and T. Chraska, Suspension Spraying Tip: High Molecular Weight Solvent, *J. Therm. Spray Technol*, 2021, **30**, p 1148–1158.

23. V. Rat, F. Mavier, and J.-F. Coudert, Electric Arc Fluctuations in DC Plasma Spray Torch, *Plasma Chemistry and Plasma Processing*, Springer, 2017, **37**(3), p 549–580.

24. P. Fauchais, M. Vardelle, S. Goutier, and A. Vardelle, Key Challenges and Opportunities in Suspension and Solution Plasma Spraying, *Plasma Chem Plasma Process*, 2015, **35**(3), p 511–525.

25. A. Dolmaire, E. Hartikainen, S. Goutier, E. Béchade, M. Vardelle, P.-M. Geffroy, and A. Joulia, Benefits of Hydrogen in a Segmented-Anode Plasma Torch in Suspension Plasma Spraying, *J Therm Spray Tech*, 2021, **30**(1–2), p 236–250.

26. R. Zhukovskii, C. Chazelas, V. Rat, A. Vardelle, and R. Molz, Predicted Anode Arc Attachment by LTE (Local Thermodynamic Equilibrium) and 2-T (Two-Temperature)

Arc Models in a Cascaded-Anode DC Plasma Spray, *Torch Journal of Thermal Spray Technology*, n.d., **1–18**.

27. R.C. Seshadri, Sanjay Sampath, Characteristics of Conventional and Cascaded Arc Plasma Spray-Deposited Ceramic Under Standard and High-Throughput Conditions, *J Therm Spray Tech*, 2019, **28**, p 690–705.

28. M. Gombault, S. Goutier, C. Chazelas, A. Vardelle, J. Escobar, S. Senani, and A. Joulia, "Effect of Particle Scale Effect on the Erosion Behavior of Cascaded Arc Plasma Spray-Deposited Coatings," *International Thermal Spray Conference*, (Quebec city, Canada), 2021.

29. S. Zimmermann, G. Mauer, K.-H. Rauwald, and J. Schein, Characterization of an Axial-Injection Plasma Spray Torch, *J Therm Spray Tech*, 2021, doi:10.1007/s11666-021-01235-6.

30. S. Xie, C. Song, Z. Yu, S. Liu, F. Lapostolle, D. Klein, C. Deng, M. Liu, and H. Liao, Effect of Environmental Pressure on the Microstructure of YSZ Thermal Barrier Coating via Suspension Plasma Spraying, *Journal of the European Ceramic Society*, 2021, **41**(1), p 535–543.

31. V. Rat and J.F. Coudert, Acoustic Stabilization of Electric Arc Instabilities in Nontransferred Plasma Torches, *Appl. Phys. Lett.*, 2010, **96**(10), p 101503.

32. M. Jadidi, M. Mousavi, S. Moghtadernejad, and A. Dolatabadi, A Three-Dimensional Analysis of the Suspension Plasma Spray Impinging on a Flat Substrate, *Journal of Thermal Spray Technology*, Springer, 2015, **24**(1), p 11–23.

33. G. Mauer, Numerical Study on Particle–Gas Interaction Close to the Substrates in Thermal Spray Processes with High-Kinetic and Low-Pressure Conditions, *Journal of thermal spray technology*, Springer, 2019, **28**(1), p 27–39.

34. A. Dolmaire, S. Goutier, M. Vardelle, P.-M. Geffroy, and A. Joulia, Investigations on Particle Behavior at the Stagnation Zone for a Suspension Particle Jet in Plasma Spray Conditions, *J Therm Spray Tech*, 2021, **30**(4), p 1001–1014.

35. D. Soysal and A. Ansar, A New Approach to Understand Liquid Injection into Atmospheric Plasma Jets, *Surface and Coatings Technology*, 2013, **220**, p 187–190.

36. P. Fauchais, M. Vardelle, S. Goutier, and A. Vardelle, Specific Measurements of In-Flight Droplet and Particle Behavior and Coating Microstructure in Suspension and Solution Plasma Spraying, *J Therm Spray Tech*, 2015, **24**(8), p 1498–1505.

37. A. Joulia, W. Duarte, S. Goutier, M. Vardelle, A. Vardelle, and S. Rossignol, Tailoring the Spray Conditions for Suspension Plasma Spraying, *J Therm Spray Tech*, 2014, doi:10.1007/s11666-014-0184-0.

38. W. Fan and Y. Bai, Review of Suspension and Solution Precursor Plasma Sprayed Thermal Barrier Coatings, *Ceramics International*, 2016, **42**(13), p 14299–14312.

39. Y. Zhao, J. Wen, F. Peyraut, M.-P. Planche, S. Misra, B. Lenoir, J. Ilavsky, H. Liao, and G. Montavon, Porous Architecture and Thermal Properties of Thermal Barrier Coatings

Deposited by Suspension Plasma Spray, *Surface and Coatings Technology*, 2020, **386**, p 125462.

40. B. Aziz, P. Gougeon, and C. Moreau, Temperature Measurement Challenges and Limitations for In-Flight Particles in Suspension Plasma Spraying, *J Therm Spray Tech*, 2017, **26**(4), p 695–707.

41. G. Mauer, N. Schlegel, A. Guignard, R. Vaßen, and O. Guillon, Effects of Feedstock Decomposition and Evaporation on the Composition of Suspension Plasma-Sprayed Coatings, *Journal of Thermal Spray Technology*, 2015, **24**(7).

42. F. Mavier, V. Rat, M. Bienia, M. Lejeune, and J.-F. Coudert, Suspension and Precursor Solution Plasma Spraying by Means of Synchronous Injection in a Pulsed Arc Plasma, *Surface and Coatings Technology*, Elsevier, 2017, **318**, p 18–27.

43. M. Vardelle, C. Trassy, A. Vardelle, and P. Fauchais, Experimental Investigation of Powder Vaporization in Thermal Plasma Jets, *Plasma Chem Plasma Process*, 1991, **11**(2), p 185–201.

44. A. Akbarnozari, F. Ben-Ettouil, S. Amiri, O. Bamber, J.-D. Grenon, M. Choquet, L. Pouliot, and C. Moreau, Online Diagnostic System to Monitor Temperature of In-Flight Particles in Suspension Plasma Spray, *J Therm Spray Tech*, 2020, **29**(5), p 908–920.

45. J. Cizek, D. Dukovsky, R. Musalek, J. Medricky, T. Tesar, F. Lukac, and T. Chraska, Suspension Spraying Tip: High Molecular Weight Solvent, *J Therm Spray Tech*, 2021, **30**(5), p 1148–1158.

46. É. Yvenou, A. Bily, F. Ben Ettouil, A. Dolatabadi, B. Davis, D. Guay, C. Moreau, and L. Roué, TiB2 Deposited on Graphite by Suspension Plasma Spray as Al Wettable Cathode, *J Therm Spray Tech*, 2021, **30**(6), p 1535–1543.

47. R.J. Adrian, Twenty Years of Particle Image Velocimetry, *Exp Fluids*, 2005, **39**(2), p 159–169.

48. O. Marchand, L. Girardot, M.P. Planche, P. Bertrand, Y. Bailly, and G. Bertrand, An Insight into Suspension Plasma Spray: Injection of the Suspension and Its Interaction with the Plasma Flow, *J Therm Spray Tech*, 2011, **20**(6), p 1310–1320.

49. X. Chen, H. Honda, S. Kuroda, H. Araki, H. Murakami, M. Watanabe, and Y. Sakka, Highly Segmented Thermal Barrier Coatings Deposited by Suspension Plasma Spray: Effects of Spray Process on Microstructure, *J Therm Spray Tech*, 2016, **25**(8), p 1638–1649.

50. L. Bianchi, A.C. Leger, M. Vardelle, A. Vardelle, and P. Fauchais, Splat Formation and Cooling of Plasma-Sprayed Zirconia, *Thin Solid Films*, 1997, **305**(1–2), p 35–47.

51. S. Goutier, M. Vardelle, and P. Fauchais, Last Developments in Diagnostics to Follow Splats Formation during Plasma Spraying, *J. Phys.: Conf. Ser.*, 2011, **275**, p 012003.

52. C. Escure, M. Vardelle, and P. Fauchais, Experimental and Theoretical Study of the Impact of Alumina Droplets on Cold and Hot Substrates, *Plasma Chemistry and Plasma Processing*, 2003, **23**(2), p 185–221.

53. N.Z. Mehdizadeh, M. Lamontagne, C. Moreau, S. Chandra, and J. Mostaghimi, Photographing Impact of Molten Molybdenum Particles in a Plasma Spray, *Journal of Thermal Spray Technology*, 2005, **14**(3), p 354–361.

54. A. McDonald, M. Lamontagne, C. Moreau, and S. Chandra, Impact of Plasma-Sprayed Metal Particles on Hot and Cold Glass Surfaces, *Thin Solid Films*, 2006, **514**(1–2), p 212–222.

55. K. Shinoda, H. Murakami, S. Kuroda, S. Oki, K. Takehara, and T.G. Etoh, High-Speed Thermal Imaging of Yttria-Stabilized Zirconia Droplet Impinging on Substrate in Plasma Spraying, *Appl. Phys. Lett.*, 2007, **90**(19), p 194103.

56. G. Bidron, S. Goutier, M. Vardelle, P. Denoirjean, and P. Fauchais, Flattening Behavior of Micro- and Nano-Sized Yttria-Stabilized Zirconia Particles Plasma-Sprayed on Smooth Preheated (610 K) Nickel Substrate: Part I, *J. Phys. D: Appl. Phys.*, 2019, **52**(16), p 165201.

57. A. Joulia, G. Bolelli, E. Gualtieri, L. Lusvarghi, S. Valeri, M. Vardelle, S. Rossignol, and A. Vardelle, Comparing the Deposition Mechanisms in Suspension Plasma Spray (SPS) and Solution Precursor Plasma Spray (SPPS) Deposition of Yttria-Stabilised Zirconia (YSZ), *Journal of the European Ceramic Society*, 2014, **34**(15), p 3925–3940.

58. E. Meillot and D. Guenadou, Thermal Plasma Flow Modeling: A Simple Model for Gas Heating and Acceleration, *Plasma Chemistry and Plasma Processing*, 2004, **24**(2), p 217–238.

59. A. Vardelle, G. Mariaux, and E. Legros, MODELING OF THE TIME-DEPENDENT PHENOMENA IN A DC PLASMA SPRAY PROCESS, *High Temp Mat Proc*, 2005, **9**(1), p 71–85.

60. E. Dalir, A. Dolatabadi, and J. Mostaghimi, Modeling the Effect of Droplet Shape and Solid Concentration on the Suspension Plasma Spraying, *International Journal of Heat and Mass Transfer*, 2020, **161**, p 120317.

61. M. Baeva, T. Zhu, T. Kewitz, H. Testrich, and R. Foest, Self-Consistent Cathode–Plasma Coupling and Role of the Fluid Flow Approach in Torch Modeling, *J Therm Spray Tech*, 2021, doi:10.1007/s11666-021-01261-4.

62. R. Zhukovskii, C. Chazelas, V. Rat, A. Vardelle, and R. Molz, Predicted Anode Arc Attachment by LTE (Local Thermodynamic Equilibrium) and 2-T (Two-Temperature) Arc Models in a Cascaded-Anode DC Plasma Spray, *Torch Journal of Thermal Spray Technology*, n.d., **1–18**.

63. R. Zhukovskii, C. Chazelas, V. Rat, A. Vardelle, and R. Molz, Model of a Non-Transferred Arc Cascaded-Anode Plasma Torch: The Two-Temperature Formulation, *J. Phys. D: Appl. Phys.*, 2022, **55**(6), p 065202.

64. S.-H. Liu, J.P. Trelles, A.B. Murphy, L. Li, S.-L. Zhang, G.-J. Yang, C.-X. Li, and C.-J. Li, Numerical Simulation of the Flow Characteristics inside a Novel Plasma Spray Torch, *J. Phys. D: Appl. Phys.*, 2019, **52**(33), p 335203.

65. C. Caruyer, S. Vincent, E. Meillot, J.-P. Caltagirone, and D. Damiani, Analysis of the Unsteadiness of a Plasma Jet and the Related Turbulence, *Surface and Coatings Technology*, 2010, **205**(4), p 1165–1170.

66. G. Mariaux and A. Vardelle, 3-D Time-Dependent Modelling of the Plasma Spray Process. Part 1: Flow Modelling, *International Journal of Thermal Sciences*, 2005, **44**(4), p 357–366.

67. M. Shigeta, Turbulence Modelling of Thermal Plasma Flows, *J. Phys. D: Appl. Phys.*, 2016, **49**(49), p 493001.

68. V. Colombo, A. Concetti, and E. Ghedini, "Time Dependent 3D Large Eddy Simulation of a DC Non-Transferred Arc Plasma Spraying Torch with Particle Injections," *2007 16th IEEE International Pulsed Power Conference*, (Albuquerque, NM), IEEE, 2007, p 1565–1568, doi:10.1109/PPPS.2007.4652486.

69. Mariaux G., "Modélisation Des Écoulements Instationnaires et Génie Des Procédés," (Limoges), Limoges, 2012.

70. S.M. Javid, C. Moreau, and J. Mostaghimi, Numerical Analysis of Buckling of a Single Suspension Droplet, *J Therm Spray Tech*, 2020, **29**(3), p 344–357.

71. S. Vincent, G. Balmigere, C. Caruyer, E. Meillot, and J.-P. Caltagirone, Contribution to the Modeling of the Interaction between a Plasma Flow and a Liquid Jet, *Surface and Coatings Technology*, 2009, **203**(15), p 2162–2171.

72. C. Caruyer, S. Vincent, E. Meillot, and J.-P. Caltagirone, Modeling the First Instant of the Interaction between a Liquid and a Plasma Jet with a Compressible Approach, *Surface and Coatings Technology*, 2010, **205**(4), p 974–979.

73. E. Dalir, A. Dolatabadi, and J. Mostaghimi, Modeling of Suspension Plasma Spraying Process Including Arc Movement Inside the Torch, *J Therm Spray Tech*, 2019, **28**(6), p 1105–1125.

74. C. Marchand, A. Vardelle, G. Mariaux, and P. Lefort, Modelling of the Plasma Spray Process with Liquid Feedstock Injection, *Surface and Coatings Technology*, 2008, **202**(18), p 4458–4464.

75. S. Vincent, E. Meillot, C. Caruyer, and J.-P. Caltagirone, Modeling the Interaction between a Thermal Flow and a Liquid: Review and Future Eulerian-Lagrangian Approaches, *OJFD*, 2018, **08**(03), p 264–285.

76. I. Gulyaev, Phenomenological Model of the Suspension Droplets Evaporation in a Plasma Flow Considering Different Mass Transfer Mechanisms, *Surface and Coatings Technology*, 2020, **404**, p 126454.

77. A. Farrokhpanah, T.W. Coyle, and J. Mostaghimi, Numerical Study of Suspension Plasma Spraying, *J Therm Spray Tech*, 2017, **26**(1–2), p 12–36.

78. X. Chen and E. Pfender, Behavior of Small Particles in a Thermal Plasma Flow, *Plasma Chem Plasma Process*, 1983, **3**(3), p 351–366.

79. K. Zhang, H. Xiong, and X. Shao, Dynamic Modeling of Micro- and Nano-Sized Particles Impinging on the Substrate during Suspension Plasma Spraying, *J. Zhejiang Univ. Sci. A*, 2016, **17**(9), p 733–744.

80. S.M. Javid, C. Moreau, and J. Mostaghimi, A Three-Dimensional Analysis of Drying of a Single Suspension Droplet in High Rate Evaporation Processes, *International Journal of Heat and Mass Transfer*, 2020, **157**, p 119791.

81. S. Ghorui, Unique Aspects of Thermal Plasma Torches and Reactor Design for Process Applications, *IEEE Trans. Plasma Sci.*, 2021, **49**(2), p 578–596.

82. F. Girard, E. Meillot, S. Vincent, J.P. Caltagirone, and L. Bianchi, Contributions to Heat and Mass Transfer between a Plasma Jet and Droplets in Suspension Plasma Spraying, *Surface and Coatings Technology*, 2015, **268**, p 278–283.

83. L. Pawlowski, Suspension and Solution Thermal Spray Coatings, *Surface and Coatings Technology*, 2009, **203**(19), p 2807–2829.

84. R. Rampon, O. Marchand, C. Filiatre, and G. Bertrand, Influence of Suspension Characteristics on Coatings Microstructure Obtained by Suspension Plasma Spraying, *Surface and Coatings Technology*, Elsevier, 2008, **202**(18), p 4337–4342.

85. F. Tarasi, E. Alebrahim, A. Dolatabadi, and C. Moreau, A Comparative Study of YSZ Suspensions and Coatings, *Coatings*, Multidisciplinary Digital Publishing Institute, 2019, **9**(3), p 188.

86. K. Hollis and R. Neiser, Particle Temperature and Flux Measurement Utilizing a Nonthermal Signal Correction Process, *Journal of Thermal Spray Technology*, 1998, **7**(3), p 392–402.

87. D. Wroblewski, G. Reimann, M. Tuttle, D. Radgowski, M. Cannamela, S.N. Basu, and M. Gevelber, Sensor Issues and Requirements for Developing Real-Time Control for Plasma Spray Deposition, *J Therm Spray Tech*, 2010, **19**(4), p 723–735.

88. K. Bobzin, W. Wietheger, M.A. Knoch, and S.R. Dokhanchi, Estimation of Particle Mass Flow Rate in Free Jet Using In-Flight Particle Diagnostics in Plasma Spraying, *J Therm Spray Tech*, 2020, **29**(5), p 921–931.

89. A. Akbarnozari, S. Amiri, A. Dolatabadi, and C. Moreau, Analysis of Scattering Light from In-Flight Particles in Suspension Plasma Spray for Size Measurement, *J Therm Spray Tech*, 2019, **28**(4), p 678–689.

90. S. Guessasma, Z. Salhi, G. Montavon, P. Gougeon, and C. Coddet, Artificial Intelligence Implementation in the APS Process Diagnostic, *Materials Science and Engineering: B*, 2004, **110**(3), p 285–295.

91. Marie-Pierre Planche, Taikai Liu, Sihao Deng, and Ghislain Montavon, Development of an Emulator for the Plasma Process Control, *JMEA*, 2015, **5**(1), doi:10.17265/2159-5275/2015.01.002.

92. T. Liu, M.P. Planche, A.F. Kanta, S. Deng, G. Montavon, K. Deng, and Z.M. Ren, Plasma Spray Process Operating Parameters Optimization Based on Artificial Intelligence, *Plasma Chem Plasma Process*, 2013, **33**(5), p 1025–1041.

93. H. Wu, S. Liu, Y. Zhang, H. Liao, R.-N. Raoelison, and S. Deng, New Process Implementation to Enhance Cold Spray-Based Additive Manufacturing, *J Therm Spray Tech*, 2021, **30**(5), p 1284–1293.